View Online

Viologen-based redox-switchable anion-binding receptors†

Ramu Kannappan,[a] Christophe Bucher,*[a] Eric Saint-Aman,*[a] Jean-Claude Moutet,[a] Anne Milet,[b] Mircea Oltean,[b] Estelle Métay,[c] Stéphane Pellet-Rostaing,[c] Marc Lemaire[c] and Carole Chaix[d]

Received (in Montpellier, France) 14th December 2009, Accepted 8th April 2010
First published as an Advance Article on the web 28th May 2010
DOI: 10.1039/b9nj00757a

Published on 28 May 2010 on http://pubs.rsc.org | doi:10.1039/B9NJ00757A
Downloaded by Technische Universitat Braunschweig on 21 October 2010

A series of viologen-based receptors have been synthesized and their anion-binding properties have been investigated by-NMR, UV-visible spectroscopy, electrochemistry and X-ray diffraction analyses. Linking two positively charged viologens through a propyl chain promotes a remarkable chelate-like binding of chlorides revealed by ^{1}H-NMR spectroscopy. Of all the anionic species investigated, only fluoride is detectable by the naked eye and by electrochemical methods. The reduction-triggered formation of a π-dimer from two viologen-based cation radicals was also investigated by electrochemical and spectroelectrochemical methods and by theoretical calculations.

Introduction

The design of artificial receptors capable of recognizing/sensing anionic species in polar media still remains a challenging task, with many potential applications in biology, medicine or environmental science.[1–4] A wide range of synthetic anion receptors have yet been designed in efforts to improve binding strengths, selectivities and signaling processes.[5–10] These investigations have demonstrated that efficient transductions of molecular recognition events require the intimate association between binding and signalling moieties into multicomponent architectures.[11] Chromogenic chemosensors are known to be particularly attractive systems allowing low detection limits, but redox analogs conversely require much simpler technologies to simultaneously activate/deactivate and enable recognition processes.[12] The anion-binding properties of polyammonium derivatives are particularly well recognized, and one finds numerous examples of saturated polyammonium compounds efficiently complexing anionic species in highly competitive media.[13] Their unusual anion-binding properties arise from favourable combinations of structurating effects, electrostatic forces and hydrogen bonds but the lack of intrinsic electrochemical or photochemical read-out signals usually requires the use of potentiometric or microcalorimetric measurements to follow and characterize their interactions with anions.

Ammoniums deriving from conjugated heterocycles such as pyridine, imidazole, pyrimidine, pyrazine or purine,[2] whilst keeping their efficient anion-binding capabilities, may conversely exhibit well defined photochemical and electrochemical signatures which could be advantageously used as transduction signals of anion-binding processes. Among this class of molecules, viologens have attracted considerable interest due to their wide range of properties finding potential applications in analytical chemistry, in solar energy conversion, in molecular electronics, electrochromic devices or in agriculture.[14] In particular, their ability to form charge-transfer complexes with electron-rich aromatic species has been exploited by Stoddart and co-workers to produce self-assembled interlocked supramolecular materials.[15,16] However, these positively charged, electron-deficient derivatives have seldom been considered as key binding and/or signaling elements in artificial molecular receptors,[17–21] although their photochemical and electrochemical signatures have been shown to be highly sensitive to their substitution pattern and immediate environment.[22–33]

In the present article, we report the syntheses and detailed physico-chemical characterizations of viologen-based anion receptors. The halide-binding properties were estimated by-NMR, UV-visible spectroscopy and by electrochemistry. The redox-triggered formation of an intramolecular π-dimer was also investigated by electrochemical and spectroelectrochemical methods, and essential structural and mechanistic information on a redox-triggered tweezer-like motion was obtained by theoretical calculations.

Experimental

General methods

^{1}H-NMR and ^{13}C-NMR spectra were recorded on Bruker 300 or 400 MHz spectrometers. ^{1}H chemical shifts (ppm) were referenced to residual solvent peaks. IR spectra were recorded using KBr pellets on a Perkin-Elmer spectrophotometer in the

[a] *Laboratoire de Chimie Inorganique Rédox, Département de Chimie moléculaire, UMR-5250, ICMG FR-2607, Institut de Chimie Moléculaire de Grenoble, FR CNRS 2607, Université Joseph Fourier, BP 53, 38041 Grenoble Cédex 9, France*
[b] *Laboratoire de Chimie Théorique, Département de Chimie moléculaire, UMR-5250, ICMG FR-2607, Institut de Chimie Moléculaire de Grenoble, FR CNRS 2607, Université Joseph Fourier, BP 53, 38041 Grenoble Cédex 9, France*
[c] *Institut de Chimie et Biochimie Moléculaires et Supramoléculaires (ICBMS-UMR5246), Université Claude Bernard Lyon 1, Domaine Scientifique de la Doua, 43 Boulevard du 11 Novembre 1918, 69622 Villeurbanne Cedex, France*
[d] *UMR des Sciences Analytiques (UMR5180), Université Claude Bernard, Bât. J. Raulin, 69622 Villeurbanne Cedex, France*

† Electronic supplementary information (ESI) available: Spectra and additional experimental details. CCDC reference numbers 772917–772919. For ESI and crystallographic data in CIF or other electronic format see DOI: 10.1039/b9nj00757a

View Online

Published on 28 May 2010 on http://pubs.rsc.org | doi:10.1039/B9NJ00757A
Downloaded by Technische Universitat Braunschweig on 21 October 2010

4000–400 cm^{-1} region. UV-vis spectra were recorded on an MCS 500 UV-NIR Zeiss spectrophotometer using conventional quartz cells or all-quartz immersion probes (Hellma Inc.). Elemental analyses (C, H and N) were carried out on a Perkin-Elmer 240 analyzer. ESI positive mode spectra were recorded with an Esquire 3000 Plus, Bruker Daltonics.

All chemicals were used as received unless described otherwise. 4,4-Dipyridyl (98%) and iodoacetamide (98%) were purchased form Acros chemicals. Anhydrous acetonitrile and DMF were purchased from Rathburn Inc. and Acros, respectively. 1-methyl-4-(4′-pyridyl)pyridinium iodide and 1,1′-dimethyl-4,4′-bipyridinium bis(hexafluorophosphate) were synthesized according to literature procedures.[34,35] 1-(Carbamoylmethyl)-1′-methyl-4,4′-bipyridinium bis(hexafluorophosphate) was prepared through a modification of a published procedure.[36]

Cyclic voltammetry (CV), differential pulse voltammetry (DPV) and voltammetry with rotating disc electrodes (RDEs) were recorded using a CH-600 potentiostat (CH-instrument). All analytical experiments were conducted under an argon atmosphere (glove box or argon stream) in a standard one-compartment, three-electrode electrochemical cell. Tetra-*n*-butylammonium perchlorate (TBAP) or tetra-*n*-butylammonium hexafluorophosphate ($TBAPF_6$). were used as supporting electrolytes (0.1 M) in non-aqueous (CH_3CN, DMF) media. An ohmic drop compensation was performed when using cyclic voltammetry. CH-instrument vitreous carbon (∅ = 3 mm) or platinum (∅ = 2 mm) working electrodes were polished with 1 μm diamond paste before each recording. Standard sweep rates of 50 mV s^{-1} and 10 mV s^{-1} were used in all DPV and RDE experiments, respectively. Voltamperometry with a rotating disk electrode (RDE) was carried out with a radiometer at a rotation rate of 500 rad min^{-1} using a glassy carbon RDE tip (∅ = 3 mm).

Spectroelectrochemical measurements were carried out in a glove box with a standard potentiostat coupled to an MCS 500 UV-NIR Zeiss spectrophotometer using a 1 mm all-quartz immersion probes. Electrolyses were conducted at 25 °C using a cylinder-shaped platinum gauze working electrode and a large piece of carbon felt as a counter-electrode isolated from the electrolytic solution through an ionic bridge. A CH instrument $Ag|AgNO_3$ (10^{-2} M + TBAP 10^{-1} M in CH_3CN) was used as a reference electrode.

The anion-sensing properties of **1** and **2** were investigated by cyclic voltammetry (CV), differential pulsed voltammetry (DPV), and with rotating disk electrodes (RDEs). In a typical experiment, changes in the electrochemical signatures of a 1×10^{-3} M solution (3 ml, 0.1 M TBAP) of a given receptor were monitored upon progressively adding increasing amounts of targeted anions (as their tetra-*n*-butylammonium salts) dissolved in the same electrolyte.

Syntheses

1-Carbamoylmethyl-4-(4′-pyridyl)pyridinium iodide [3·I]. To a stirred dichloromethane solution (100 ml) of 4,4′-dipyridyl (3.12 g, 20 mmol) was added iodoacetamide (2.5 g, 14 mmol) and the mixture was stirred under reflux for 24 h. After cooling, the yellow precipitate of **3**·I was filtered, washed with 10 ml of diethyl ether and dried *in vacuo*. Yield: 57%; ^{1}H-NMR (300 MHz, DMSO-d_6) δ: 9.12 (d, J = 6.6 Hz, 2H, Ar), 8.87 (d, J = 6.0 Hz, 2H, Ar), 8.65 (d, J = 6.6 Hz, 2H, Ar), 8.05 (d, J = 6.0 Hz, 2H, Ar), 8.05 (s, NH), 7.71 (s, NH) 5.44 (s, 2H, Ar-N-CH_2). ^{13}C-NMR (75 MHz, DMSO-d_6) δ: 164.7, 151.4, 149.6, 145.4, 139.5, 123.4, 120.6, 59.8; IR (KBr, cm^{-1}); 3265 (m) 3032 (s), 1700 (s), 1639 (s), 1603 (m), 1399 (s), 1311 (m), 1225 (m), 812 (s). MS (ESI): m/z 213.9 [M + 1]. Calcd for $C_{12}H_{12}IN_3O$: C, 42.24; H, 3.54; N, 12.32. Found: C, 42.45; H, 3.80; N, 12.49.

1-(Carbamoylmethyl)-1′-methyl-4,4′-bipyridinium bis(hexafluorophosphate) [1·(PF_6)$_2$]. This derivative was prepared through a modification of a published procedure.[36]

To a solution of 1-methyl-4-(4′-pyridyl) pyridinium iodide (1.49 g, 5 mmol) in acetonitrile stirred under an argon atmosphere was added iodoacetamide (0.92 g, 5 mmol). The reaction mixture was heated under reflux for 24 h. After cooling, the reddish precipitate was filtered and washed with diethyl ether. The crude solid was dissolved in a minimum of water and saturated aqueous KPF_6 solution was added dropwise to the resulting solution until observing a precipitate which was filtered and washed with water and diethyl ether to afford **1**·(PF_6)$_2$ as a pale yellow solid. Yield: 91%; ^{1}H-NMR (300 MHz, DMSO-d_6) δ: 9.25 (d, J = 6.6 Hz, 4H, Ar), 8.76 (d, J = 6.0 Hz, 4H, Ar), 8.08 (s, NH), 7.75 (s, NH), 5.49 (s, 2H, Ar-N-CH_2), 4.44 (s, 3H, Ar-CH_3). ^{13}C-NMR (75 MHz, DMSO-d_6) δ: 165.8, 149.1, 148.3, 147.2, 146.5, 126.1, 125.8, 61.5, 47.9; IR (KBr, cm^{-1}); 3032 (s), 1713 (s), 1640 (s), 1603 (m), 1392 (s), 1329 (m), 1195 (m), 806 (s). MS (ESI): m/z 374 $[M - PF_6]^+$. Calcd for $C_{13}H_{15}N_3{\cdot}2PF_6$: C, 30.08; H, 2.92; N, 8.1. Found: C, 30.08; H, 3.11; N, 7.95.

1,1′′-(1,3-Propanediyl)bis(1′-carbamoylmethyl)-4,4′-bipyridinium tetrakis(hexafluorophosphate) [2·(PF_6)$_4$]. To a solution of **3**·I (0.34 g, 4 mmol) in dry DMF was added dropwise 1,3-dibromopropane (0.2 ml, 2 mmol). The reaction mixture was refluxed for 2 days. After cooling, the brown precipitate was filtered, washed with cold DMF and dried. The crude solid was dissolved in a minimum of water and saturated aqueous KPF_6 solution was added dropwise to the resulting solution until a precipitate formed. This was filtered off, and washed with water and diethyl ether to afford the product as a white solid. Yield: 32%. ^{1}H-NMR (300 MHz, DMSO-d_6) δ: 9.32 (dd J = 6.8, 6.6 Hz, 8H, Ar), 8.82 (dd, J = 6.6, 6.0 Hz, 8H, Ar), 8.10 (s, NH, 2H), 7.77 (s, NH, 2H), 5.50 (s, 4H, N-CH_2CO), 4.84 (m, 4H, N-CH_2), 2.79 (m, 2H). ^{13}C-NMR (75 MHz, DMSO-d_6) δ: 165.8, 148.9, 147.3, 146.0, 126.6, 125.8, 61.6, 57.6, 31.4. IR (KBr, cm^{-1}); 3454 (m), 1717 (m), 1693 (s), 1641 (s), 1451 (m), 832 (s), 558 (s). MS (ESI): m/z 905 $[M - PF_6]^+$. Calcd for $C_{27}H_{30}N_6O_2P_4F_{24}$: C, 30.88; H, 2.88; N, 8.01. Found: C, 30.50; H, 2.61; N, 7.92.

X-Ray diffraction

Data collections were scanned in ϕ and ω mode on a Bruker AXS-Enraf-Nonius KappaCCD diffractometer using Mo Kα radiation (λ = 0.71073 Å). Monocrystals of **1**·(PF_6)$_2$ could be obtained in DMSO by slow vapor phase diffusion

 This journal is © The Royal Society of Chemistry and the Centre National de la Recherche Scientifique 2010

View Online

of diethyl ether. The bis-viologen species were crystallized as the iodide or chloride salts by liquid-phase diffusion of tetra-*n*-butylammonium iodide or chloride in an acetonitrile solution of **2**·$(PF_6)_4$.

Crystal data for [**1**·$(PF_6)_2$], $C_{13}N_3O_1F_{12}P_2H_{15}$: orthorhombic. *Pbca*. a = 23.589(4) Å, b = 19.661(3) Å, c = 8.559(2) Å, V = 3969.5(13) Å^3. Z = 8. D = 1.737 g cm^{-3}. λ = 1.54178 Å. $F(000)$ = 2080.00. Θ range = 3.5–75°. 4609 measured reflections, 4097 independent reflections, 2332 reflections with [$I > 1.3\sigma(I)$]. 293 parameters. Reflection/parameter ratio: 8.1. $R_1[I > 1.5\sigma(I)]$ = 7.17%. wR_2 = 11.52%. GOF = 2.0 refined against F.

Crystal data for [**2**·DMSO·$(I)_4$], $C_{29}H_{36}N_6O_3I_4S$ or $C_{27}H_{30}N_6O_2$ $(CH_3)_2SO$·$(I^-)_4$: monoclinic. *C*2/*c*. a = 18.430(1) Å, b = 9.537(3) Å, c = 20.999(4) Å, β = 91.64(2)°, V = 3689.4(8) Å^3. Z = 4. D = 1.902 g cm^{-3}. λ = 0.71073Å. $F(000)$ = 2016.00. Θ range = 2–30°. 20 286 measured reflections, 4824 [R_{int} = 0.11] independent reflections, 3453 reflections with [$I > 2.0\sigma(I)$]. 200 parameters. Reflection/parameter ratio: 17.3. $R_1[I > 2.0\sigma(I)]$ = 3.65%. wR_2 = 4.47%. GOF = 1.891 refined against F.

Crystal data for [**2**·$(H_2O)_{0.5}$·$DMSO_{0.55}$·$(Cl)_4$], $C_{28.10}H_{35.3}Cl_4N_6O_{3.55}S_{0.55}$: monoclinic. *C*2/*c*. a = 15.533(5) Å, b = 12.135(2) Å, c = 36.868(2) Å, β = 99.88(2)°, V = 6846(3) Å^3, Z = 8, D = 1.306 g cm^{-3}, λ = 0.71073 Å. $F(000)$ = 2808.80. Θ range = 1–25°. 26 459 measured reflections, 5915 [R_{int} = 0.09] independent reflections, 3083 reflections with [$I > 2.0\sigma(I)$]. 385 parameters. Reflection/parameter ratio: 8.0. $R_1[I > 2.0\sigma(I)]$ = 8.99%. wR_2 = 12.50%. GOF = 1.98 refined against F.

Computational details

The quantum chemistry calculations were carried out with both the CP2KQuickStep program and the Gaussian03[37] program. With this latter code, we used the BLYP, B3LYP,[38] B3LYP-CP[39] (Corrected Potential) and MP2[40] functional with the 6-31+G(d,p)[41,42] basis sets.

Solvent effects were evaluated using the polarizable continuum model (PCM)[43–46] in which the cavity is created *via* a series of overlapping spheres.

The *ab initio* Born–Oppenheimer dynamics calculations were performed using the CP2K-QuickStep program CP2K, (http://cp2k.berlios.de, 2000–2009)[47] at the DFT level with the BLYP[48,49] – D[50] functional. QuickStep is an implementation of the Gaussian Plane Waves (GPW) method based on the Kohn–Sham formulation of density functional theory (DFT). It is a hybrid method using a linear combination of Gaussian-type orbitals to describe the Kohn–Sham orbitals, whereas an auxiliary plane waves basis set is employed to expand the electronic charge density.

The basis set used was a double-ζ valence set of Gaussian orbitals[51] in conjunction with the Goedecker–Teter–Hutter[52–54] pseudopotentials. The auxiliary PW basis set was defined by a cubic box of 25 Å^3 and by a density cutoff of 360 Ry. Metadynamics[55,56] has been used to overcome the problem of observing rare events in conventional molecular dynamics and determining the energy barrier of our system. Further computational details are given as ESI†.

Results and discussion

Syntheses

Both viologen derivatives $\mathbf{1}^{2+}$ and $\mathbf{2}^{4+}$ were synthesized by stepwise quaternization of 4,4′-bipyridine with iodoacetamide, methyl iodide and/or 1,3-dibromopropane (Scheme 1). PF_6^- salts of $\mathbf{1}^{2+}$, $\mathbf{2}^{4+}$ and $\mathbf{4}^{2+}$ were easily obtained, from the iodide precursors, by precipitation in water through anion metathesis. Elemental and spectroscopic analyses were consistent with each targeted receptors. It needs to be mentioned that $\mathbf{2}^{4+}$ could also be obtained upon following the reverse quaternization sequence, starting with 1,3-dibromopropane and subsequently introducing the amide functionality.

The ^{1}H-NMR spectra of **1**·$(PF_6)_2$ and **2**·$(PF_6)_4$ recorded in deuterated DMSO showed similar features with two singlets at 4.4 and 5.5 ppm, attributed to the –NCH_3 and –NCH_2CO– fragments, two amide NH-based singlets at 7.8 and 8.1 ppm and four doublets between 8.7 and 9.3 ppm attributed to the pyridinium moieties. The accurate attribution of all signals (Fig. 1) has been achieved using COSY and HMQC correlation maps (see ESI†). Both doublets attributed to the H_f and H_c protons in $\mathbf{2}^{4+}$ could especially be distinguished through the observation of correlations with the adjacent methylenic protons (N^+CH_2CO *vs.* $N^+CH_2CH_2$).

Signals attributed to aliphatic protons are not shown on Fig. 1. The H_g protons are observed as a singlet at *ca.* 5.5 ppm on the spectrum of $\mathbf{1}^{2+}$ and $\mathbf{2}^{4+}$ whereas the propyl linker (H_i, H_j) in $\mathbf{2}^{4+}$ appears as two multiplets at 4.8 and 2.8 ppm.

Both species were further characterized in the solid state by X-ray diffraction analysis. As shown on Fig. 2, the viologen fragments linked through a propyl linker in $\mathbf{2}^{4+}$ form an angle close to 90° defining an open positively charged cavity. The pyridine subunits in the same viologen fragment are not fully coplanar but slightly twisted, by around 13° in $\mathbf{2}^{4+}$ and 31° in $\mathbf{1}^{2+}$. In each case, the CNO amide fragments define planes forming a 90° angle with the closest pyridinium rings.

Electrochemistry

The electrochemical signatures of **1**·$(PF_6)_2$ and **2**·$(PF_6)_4$ were investigated in CH_3CN, DMF and H_2O at 1 × 10^{-3} M using cyclic voltammetry (CV), differential pulsed voltammetry (DPV) and voltammetry with rotating disc electrodes (RDEs). The CV curves of both species exhibit similar patterns showing both well-known[14] consecutive viologen-centered reversible reductions (eqn (1) and (2), Fig. 3 and ESI†). In agreement with the electron-withdrawing character of amide fragments, the first reduction potentials of $\mathbf{1}^{2+}$ and $\mathbf{2}^{4+}$ are significantly shifted towards less negative values compared to the reference compound $\mathbf{4}^{2+}$ (Table 1). The substantial shift observed between the first reduction potential of $\mathbf{1}^{2+}$ and $\mathbf{2}^{4+}$ might be attributed to their different charges and/or to the existence of a chemical reaction coupled to the electron transfer in $\mathbf{2}^{4+}$. This particular aspect will be discussed in the following paragraph. The second reduction happens to be far less influenced by the viologen substitution pattern. In aqueous media, the adsorption of the neutral forms $\mathbf{1}^0$ and $\mathbf{2}^0$ on the electrode surface was demonstrated by the observation of intense stripping CV-peaks on the reverse scan. Solvent effects

Published on 28 May 2010 on http://pubs.rsc.org | doi:10.1039/B9NJ00757A
Downloaded by Technische Universitat Braunschweig on 21 October 2010

View Online

Downloaded by Technische Universitat Braunschweig on 21 October 2010
Published on 28 May 2010 on http://pubs.rsc.org | doi:10.1039/B9NJ00757A

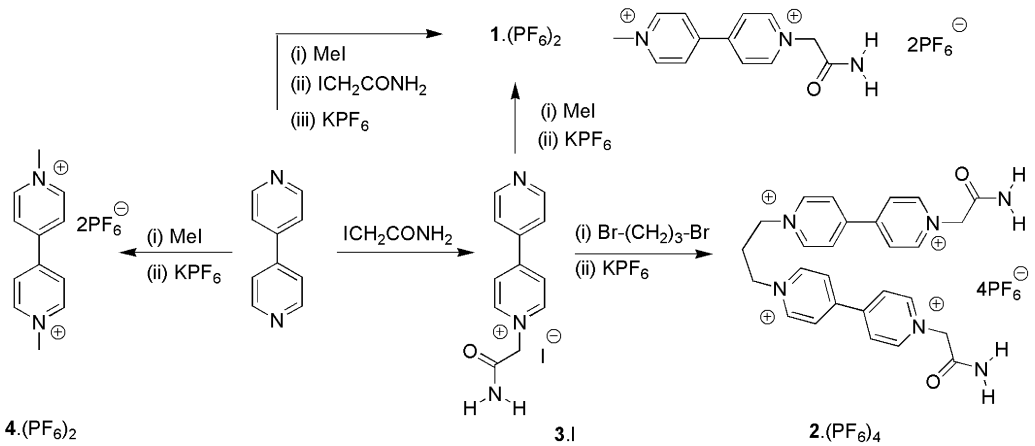

Scheme 1 Stepwise syntheses of **1**·$(PF_6)_2$, **2**·$(PF_6)_4$, **3**·I and **4**·$(PF_6)_2$.

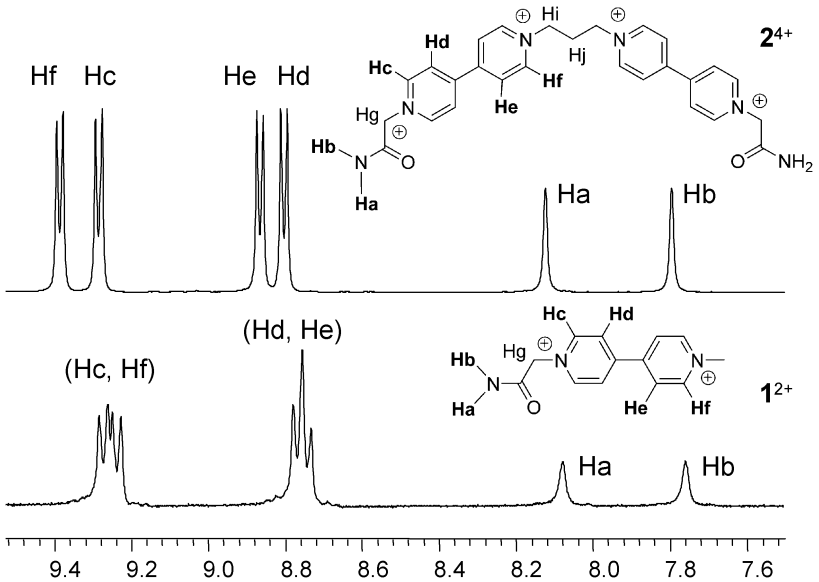

Fig. 1 ^{1}H-NMR spectra of **1**·$(PF_6)_2$ and **2**·$(PF_6)_4$ from 7.5 to 9.5 ppm (DMSO-d_6, 300 MHz).

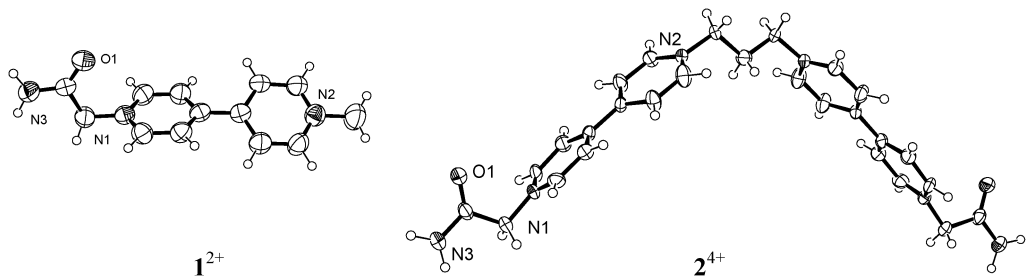

Fig. 2 ORTEP[57] views of **1**·$(PF_6)_2$ and [**2**·DMSO·$(I)_4$] showing the heteroatom-labeling scheme. Solvent molecules and counter-anions have been omitted for clarity. Ellipsoids are drawn at a 50% probability level for $\mathbf{1}^{2+}$ and 45% for $\mathbf{2}^{4+}$.

were furthermore clearly shown through the half-wave potential shifts ($\Delta E_{1/2}$) of the first reduction process between acetonitrile and DMF electrolytes.

The electrochemical behaviour of molecules with multiple redox centres has already been thoroughly investigated.[58,59] It has been demonstrated that electron transfers to or from molecules containing identical, non-interacting, electroactive centres should yield a single current–potential CV curve similar to that observed with a single electroactive centre (ΔE_p = 58 mV at 25 °C) but with a magnitude determined by the total number of redox centres. When each centre is characterized by the same standard potential E^0_m, and adheres to the Nernst equation independently of the oxidation state of any of the other centres in the molecule, it is possible to

 This journal is © The Royal Society of Chemistry and the Centre National de la Recherche Scientifique 2010

View Online

Published on 28 May 2010 on http://pubs.rsc.org | doi:10.1039/B9NJ00757A
Downloaded by Technische Universitat Braunschweig on 21 October 2010

$$V^{2+} + e \rightleftharpoons V^{+\bullet} \quad (E^0_1) \qquad (1)$$

$$V^{+\bullet} + e \rightleftharpoons V^0 \quad (E^0_2) \qquad (2)$$

$$V^{2+}\text{---}V^{2+} + e \rightleftharpoons V^{2+}\text{---}V^{+\bullet} \quad (E^0_{1\_1}) \qquad (3)$$

$$V^{2+}\text{---}V^{+\bullet} + e \rightleftharpoons V^{+\bullet}\text{---}V^{+\bullet} \quad (E^0_{1\_2}) \qquad (4)$$

$$V^{+\bullet}\text{---}V^{+\bullet} \rightleftharpoons (V\text{---}V)^{2+}_{dim} \quad (K_{dim}) \qquad (5)$$

$$2\ V^{2+}\text{---}V^{+\bullet} \rightleftharpoons V^{+\bullet}\text{---}V^{+\bullet} + V^{2+}\text{---}V^{2+} \quad (K_d) \qquad (6)$$

Fig. 3 Successive one-electron reductions of a generic viologen (eqn (1) and (2)). Decomposition of the first reduction processes in linked bis-viologen species (eqn (3) and (4)) and their potential coupled reactions (dimerization (5) and disproportionation (6)).

Table 1 Half-wave potential ($E_{1/2}$) measured by cyclic voltammetry (100 mV s^{-1}) on platinum electrodes in DMF or CH_3CN electrolytes (0.1 M $TBAPF_6$). ΔE_p values[a] were measured at low scan rate (20 mV s^{-1}). $\Delta E^0 = E^0_{1\_1} - E^0_{1\_2}$ was estimated using a method established by Richardson *et al.*[69]

	Solvent	$(E_{1/2})_1$	$(E_{1/2})_2$	$(\Delta E_p)_1$	ΔE^0	K_d ($\times 10^{-3}$)
4·$(PF_6)_2$	DMF	−830	−1200	68	—	—
1·$(PF_6)_2$	CH_3CN	−692	−1097	60	—	—
	DMF	−797	−1175	61	—	—
2·$(PF_6)_4$	CH_3CN	−580	−1123	38	27	348
	DMF	−714	−1204	48	17	515

[a] V *vs.* Ag/Ag^+ (10^{-2} M). $E_{1/2\ (Fc/Fc+)} = 70$ mV in DMF. $\log_{10}(K_d) = -\Delta E^0/0.059$.

calculate the formal potentials corresponding to each pair of *n* successive oxidation states of the multi-centre molecules. Considering fully non-interacting centres, the theoretical shift between both first viologen-based formal reduction potentials in $\mathbf{2}^{4+}$ ($E^0_{1\_1}$ and $E^0_{1\_2}$ on Fig. 3) should thus equal $\Delta E^0_1 = E^0_{1\_2} - E^0_{1\_1} = 35.6$ mV, although both redox processes are expected to appear as a single wave with peak potentials satisfying $\Delta E_p = 58$ mV. The lowest $(\Delta E_p)_1$ value, 38 mV, was recorded at a low scan rate in acetonitrile with $\mathbf{2}^{4+}$, in which two chemically equivalent viologens are simultaneously reduced. The low values of ΔE_p measured with $\mathbf{2}^{4+}$ in DMF or acetonitrile electrolyte are thus not in accordance with these theoretical considerations and reveal the existence of interactions between viologen radicals forming π-dimers.[60,61] Such non-covalent interactions have been observed and characterized at low temperature or high concentrations of simple viologen derivatives and in few cases at room temperature with structurally preorganized bis-viologen architectures or in confined environments.[14,62,63] Although the structural and electronic natures of this association between radical cations are still under scrutiny, the ability of bis-viologens to dimerize has yet been shown to depend on their linkers' size and flexibility. Propyl connecters have especially proved to allow efficient room-temperature formations of viologen based π-dimers.[64–68] The low $(\Delta E_p)_1$ value recorded for $\mathbf{2}^{4+}$, in which two viologens are linked by a propyl chain, is thus unambiguously related to the intramolecular association between both reduced species to form a π-dimer derivative $[\mathbf{2}^{2+}]_{dim}$. The effectiveness of this chemical process, characterized by the thermodynamic parameter K_{dim} (Fig. 3), coupled to the viologen-centered electron transfer leads to a situation in which the second viologen reduction ($E^0_{1\_2}$, Fig. 3) happens at a less negative potential than the initial one ($E^0_{1\_1}$, Fig. 3) and thus to the existence of a disproportionation equilibria with $\log K_d = -\Delta E^0/0.059$ (K_d, Fig. 3).[69]

In a first approximation, K_d as well as $E^0_{1\_2}$ and $E^0_{1\_1}$ have been estimated from the potential value $(\Delta E_p)_1$ measured by cyclic voltammetry.[69] Calculated values of ΔE^0 and K_d are thus in accordance with the existence of a disproportionation equilibrium observed with $\mathbf{2}^{4+}$ in DMF and in acetonitrile electrolyte, the displacement of the disproportionation equilibrium being attributed to the formation of an intramolecular π-dimer. This specific redox-driven π-dimerization observed in acetonitrile at room temperature contrasts with the commonly accepted belief that such association between viologen radicals should only be observed in water due to important hydrophobic contributions promoting the self-assembly of both reduced species.[14]

In situ spectroelectrochemical studies were conducted under argon in a glove box on DMF solutions of **1**·$(PF_6)_2$ and **2**·$(PF_6)_4$ (0.1 M TBAP). The one-electron bulk reduction of $\mathbf{1}^{2+}$ performed at −1 V on a platinum working electrode was followed through the large decrease in intensity of the initial absorption band at 272 nm at the expense of new bands growing at $\lambda_{max} = 399$ and 614 nm with shoulders from 530 to 730 nm (Fig. 4). The blue color and UV-vis signature of the resulting solution could be attributed[14] to the cation radical species $\mathbf{1}^{+\bullet}$. The reversibility of the reduction process at the electrolysis time scale was checked by UV-vis absorption spectroscopy and voltammetry on rotating disk electrodes upon recovering the entire signature of the initial $\mathbf{1}^{2+}$ species after back-electron transfer.

The same experiment carried out with the bis-viologen $\mathbf{2}^{4+}$ led conversely to the observation of completely different bands gradually developing at $\lambda_{max} = 366$, 543 and 866 nm (Fig. 4). The violet color and the ensuing UV-vis absorption spectrum fully coincide with the formation of the π-dimer $[\mathbf{2}^{2+}]_{dim}$, the broad absorption centered at 866 nm being a specific diagnostic

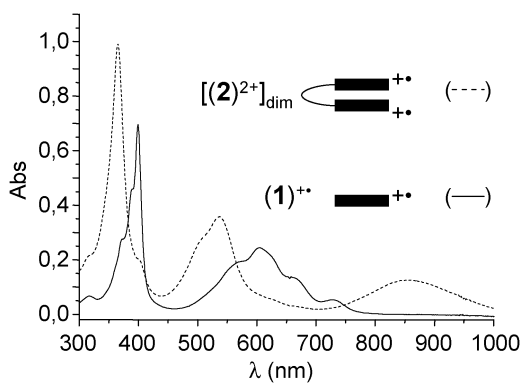

Fig. 4 UV-vis spectra recorded after exhaustive one-electron reduction per viologen in [**1**·$(PF_6)_2$] (solid line) and [**2**·$(PF_6)_4$] (dotted line) in DMF using a platinum plate working electrode whose potential was fixed at $E_{ap} = -1.0$ V (2.5×10^{-4} M in 25 ml of DMF, 0.1 M TBAP, $l = 1$ mm).

View Online

band whose energy can be directly related to the electronic-coupling term between both viologen radicals.[14,60,70]

These reduction processes are fully reversible under these conditions, as the original spectrum could be recovered by re-oxidation conducted at 0 V. It can thus be assumed that the intramolecular association in the doubly reduced $\mathbf{2}^{2+}$ species is allowed by the flexibility and size of the propyl linker.[66,68] A detailed theoretical analysis of this redox-driven self-association is reported in the last part of this article.

Halide sensing

Taking advantage of their intense and well defined physico-chemical signatures, the ability of $\mathbf{1}^{2+}$ and $\mathbf{2}^{4+}$ to bind anionic species was investigated by electrochemical methods, ^{1}H-NMR and UV-vis spectroscopy. Such viologen-amide-based receptors could indeed potentially interact with electron-rich anions through a large range of non-covalent interactions, such as ion pairing, van der Waals interactions, hydrogen bonding or donor–acceptor charge transfer processes. The simultaneous presence of cationic charges, electron-deficient pyridinium acceptors and hydrogen bond donor/acceptor amide fragments is as a matter of fact particularly suited to achieve efficient complexation/sensing of electron-rich anionic species.[2,20] As discussed above, these electron-deficient species also feature two reversible reduction processes which might advantageously be used as transduction or activation/deactivation tools. The so-called "molecular electrochemical recognition" of anionic, neutral or cationic species have been proved to be achievable in organic media using a wide range of redox-active receptors involving an intimate association between a recognition site and a signaling subunit.[11,71,72] Given the weak nature of most interaction forces involved in the 'square scheme' mechanisms describing the redox- and binding-coupled processes, the electrochemical recognition of neutral or even charged species in polar media still remains a challenging objective. Viologens are in that respect highly attracting molecular materials potentially behaving simultaneously as binding and transducing sites.

The interactions of the cationic receptors $\mathbf{1}^{2+}$ and $\mathbf{2}^{4+}$ with halides, as their tetra-*n*-butylammonium salts, were first investigated by ^{1}H-NMR in deuterated DMSO. This study could not be conducted in acetonitrile or less polar solvents due to the insolubility of most halide complexes formed with both receptors. In the case of chloride, D_2O (2% v/v) was added to ensure the complete solubility of all species at large anion concentrations.

As expected from its large size and polarizability, the addition of iodide did not induce significant changes in the ^{1}H-NMR spectrum of $\mathbf{1}\cdot(PF_6)_2$. Conversely, the addition of increasing amounts of bromide or chloride led to important shifts (Fig. 5) of only one amide-based signal attributed to NH_a, $\delta(NH_b)$ remaining constant throughout all titration experiments. The largest variation of $\delta(NH_a)$ reached 0.35 ppm in DMSO-d_6–D_2O (98:2) in the presence of an excess of chloride. The weaker but still significant concomitant displacements observed for $\delta(H_c)$ ($\Delta\delta_{max}$ = 0.11 ppm) and $\delta(H_g)$ ($\Delta\delta_{max}$ = 0.11 ppm) led us to hypothesize a cooperative binding mode in which chloride would behave as a trifurcated

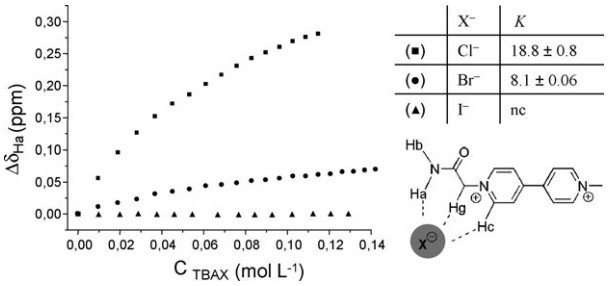

Fig. 5 ^{1}H-NMR chemical shift attibuted to NH_a as a function of the concentration of TBACl (■), TBABr (●) and TBAI (▲). Titrations were conducted with 8×10^{-3} M $\mathbf{1}\cdot(PF_6)_2$ at 400 MHz in DMSO-d_6 (TBABr and TBAI) or in DMSO-d_6–D_2O (98:2) (TBACl).

hydrogen bond[73] acceptor (Fig. 5). Fitting these experimental curves with a 1:1 binding stoichiometry allowed the estimation of the binding constant of $\mathbf{1}^{2+}$ with bromide and chloride in DMSO (Fig. 5), the significant selectivity of this simple receptor towards chloride being easily explained by a combination of strong hydrogen bonds and ion-pair-attracting effects (Fig. 5).

Similar experiments were conducted with $\mathbf{2}\cdot(PF_6)_4$, expecting that the association of two electron acceptor amide-viologen fragments would be beneficial in term of anion-binding ability. As observed for the simple analogue $\mathbf{1}\cdot(PF_6)_2$, no evidence of interaction with iodide could be seen using ^{1}H-NMR spectroscopy. In contrast, the complexation of bromide or chloride with $\mathbf{2}^{4+}$ in DMSO was clearly revealed through important displacements of two different ^{1}H-NMR signals. As expected from our preliminary investigations conducted with $\mathbf{1}^{2+}$ (Fig. 5), the involvement of both amide fragments in the anion-binding process led to a low field shift of one singlet attributed to NH_a. More surprisingly, the most important and expeditious modifications in the ^{1}H-NMR spectra were observed in the aromatic region, among the doublets attributed to the pyridinium protons. This appeared to be particularly true in the presence of bromide anions, leading simultaneously to a slight shift of the NH_a signal and to a much more important displacement of one doublet attributed to the H_f protons (Fig. 6).

A similar behaviour was observed with chloride, although the NMR shift magnitudes of both NH_a and H_f signals were far less different. The large and swift chloride-induced changes in $\delta(H_f)$ values, exclusively observed with the tetracationic bis-viologen derivative $\mathbf{2}^{4+}$, were seen as clear evidence of a structural effect allowing an unusual anion-binding mode. Moreover, the low-field shift of the H_f signal was not associated with any loss of symmetry at the NMR time-scale, as proved by the constant number of signals observed throughout the titration experiments. These findings led us to consider the formation of a poly-anionic complex, in which all the H_f protons would be involved in strong hydrogen bonds either with two anions located on each side of the receptor leading to a fully symmetric arrangement ($[\mathbf{2}\cdot X_2]^{2+}$, Fig. 7), or with only one anion pinched between two H_f protons ($[\mathbf{2}\cdot X]^{3+}$, Fig. 7) but in rapid equilibrium (at least compared to the NMR time-scale) between both possible arc-shaped binding pockets. Given the important size and rigidity of the viologen fragment, it can reasonably be assumed that the NH_a and H_f protons

Published on 28 May 2010 on http://pubs.rsc.org | doi:10.1039/B9NJ00757A
Downloaded by Technische Universitat Braunschweig on 21 October 2010

 This journal is © The Royal Society of Chemistry and the Centre National de la Recherche Scientifique 2010

View Online

Published on 28 May 2010 on http://pubs.rsc.org | doi:10.1039/B9NJ00757A
Downloaded by Technische Universitat Braunschweig on 21 October 2010

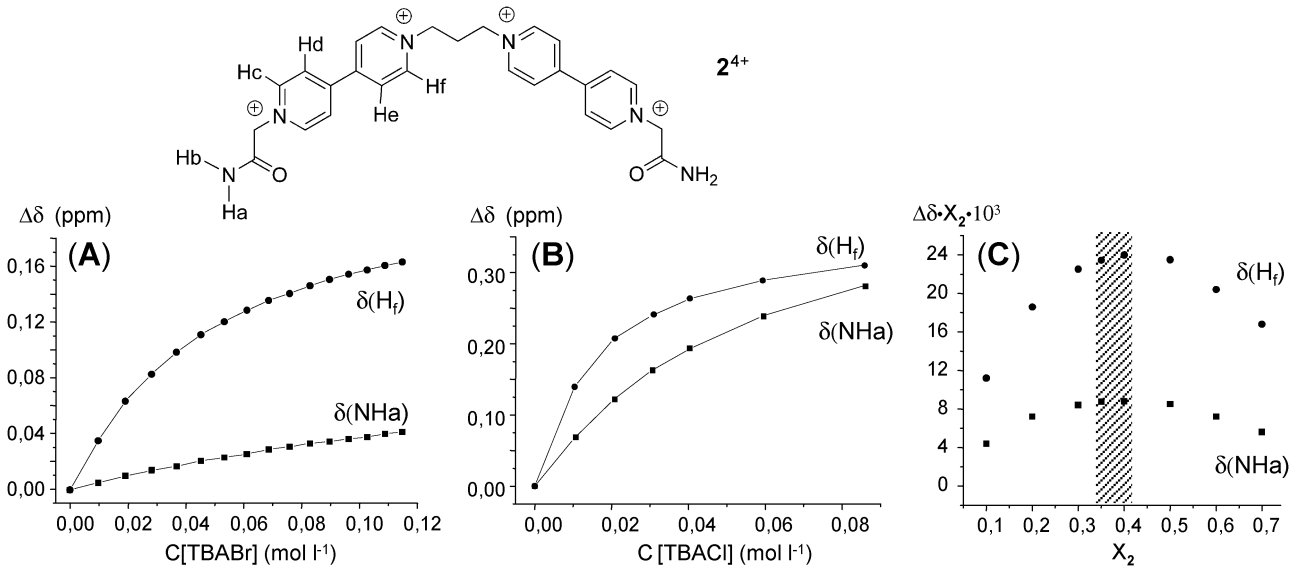

Fig. 6 ^{1}H-NMR chemical shift of H_f and NH_a recorded as a function of the concentration of (A) TBABr and (B) TBACl. (C) Continuous variation curves plotted for $\Delta\delta(H_f)$ and $\Delta\delta(NH_a)$ in DMSO solutions of $\mathbf{2}\cdot(PF_6)_4$ and TBACl. (400 MHz). The molar fraction $X_{(2)} = n_{(2)}/[n_{(2)} + n_{(Cl)}]$. Titration were conducted with 8×10^{-3} M $\mathbf{2}(PF_6)_2$.

must be involved in the complexation of different anionic guests. The shape of the anion-binding curves shown in Fig. 6(A) and (B) tells us that the binding of chloride or bromide is more efficient in the H_f-based binding pocket than through the amide groups.

This unexpected result can be explained considering unique combinations of favourable hydrogen bonding, electrostatic and chelating effects. Further information on the exact stoichiometry of the chloride complex $[\mathbf{2}_n Cl_m]^{y+}$ came from the method of continuous variations[74] leading to the Job-plot shown in Fig. 6C. Both $\Delta\delta\cdot X_{(2)}$ *versus* $X_{(2)}$ curves[75,76] plotted for H_f and NH_a showed maximum values for molar fractions $X_{(2)}$ around 0.35. This maximum, close to the theoretical value of 0.33 expected for a 1:2 binding ratio, suggests the independent complexation of two chlorides through the pyridinium H_f protons (Fig. 7, $[\mathbf{2}\cdot X_2]^{2+}$) and two more through the amide groups to yield an overall $[\mathbf{2}\cdot Cl_4]$ complex. Theoretical calculations conducted on this complex yielded a possible structure in agreement with these hypotheses. Detailed views of both chloride-binding modes found in this optimized structure are depicted in Fig. 8. This structure clearly shows the chelating effect of the positively charged viologens, hydrogen-bonded to two chloride anions located on both sides of the receptor. Each anion is in close proximity to two pyridinium H_f atoms and the three methylenic hydrogens belonging to the propyl linker, with hydrogen bond lengths ranging from 2.45 to 2.9 Å.

Experimental evidence of these interactions clearly appeared through the NMR titration, with chloride resulting in significant shifts of signals attributed to the H_i and H_j protons. All curves plotted in Fig. 8C exhibit similar shapes but significantly different amplitudes, which can be directly related to the strength of the hydrogen bonds established with chloride. The shortest H···Cl contact distance on the optimized structure was surprisingly from H_j (2.47 Å and C–Ĥ···Cl ~125°), featuring by far the less polarized C–H bond due to its relatively large distance from the positively charged pyridinium groups. The optimized structure is non-fully symmetric and features two distinct C–H_f···Cl bond lengths of 2.53 and 2.79 Å formed with favourable C–Ĥ···Cl angles of around 150°. The shape of all curves shown on Fig. 8D, related to the amide-based binding site, are notably different from those drawn with δH_f, δH_j and δH_i. In contrast to NH_b, clearly not affected by the presence of chloride in solution, the broad singlet attributed to NH_a undergoes a large shift similar to that

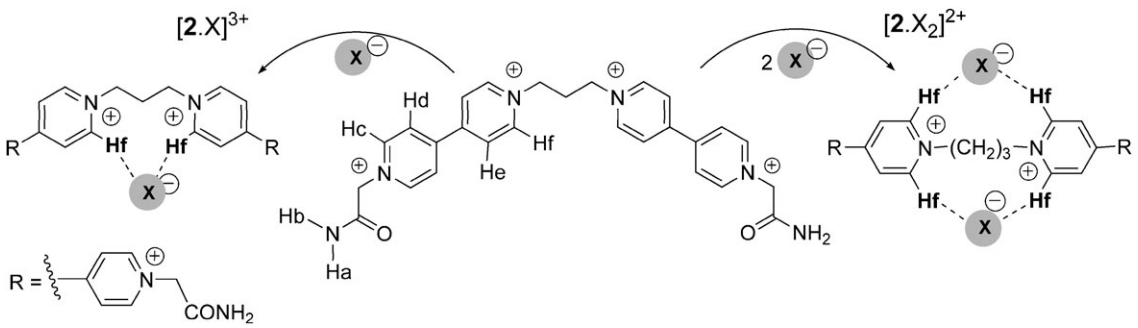

Fig. 7 Schematic representation of two potential binding modes involving the pyridinium-based H_f protons $[\mathbf{2}\cdot X]^{3+}$ and $[\mathbf{2}\cdot X_2]^{2+}$ (X = Cl^- or Br^-).

View Online

Published on 28 May 2010 on http://pubs.rsc.org | doi:10.1039/B9NJ00757A
Downloaded by Technische Universitat Braunschweig on 21 October 2010

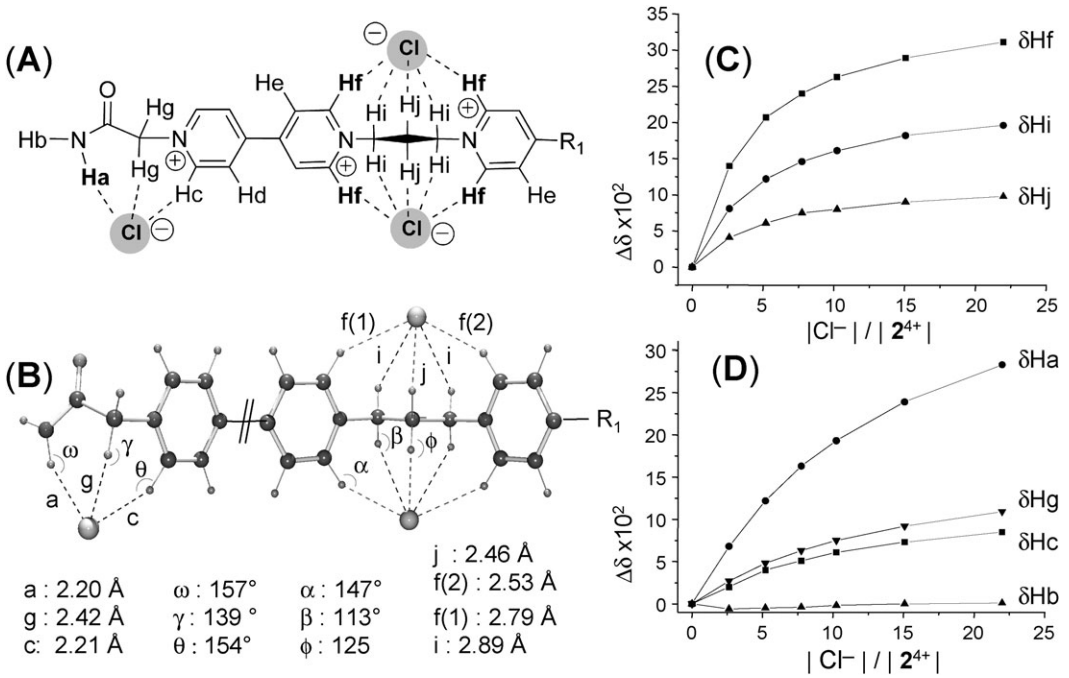

Fig. 8 (A and B) Details of both binding modes for the optimized structures of **2**·$(Cl)_4$ obtained at the B3LYP/6-31+G* calculation level. (C and D) ^{1}H-NMR chemical shifts of (C) H_f, H_i, H_j and (D) NH_a, H_g, H_c, H_b recorded as a function of the concentration of TBACl. Titration were conducted with 8×10^{-3} M **2**·$(PF_6)_2$ at 400 MHz in DMSO-d_6–D_2O (98:2).

observed with the simple analogue **1**·$(PF_6)_2$. Weaker displacements but similar curve profiles (Fig. 8D) were also observed with δH_g and δH_c involved in the same binding process, as seen on the optimized structure showing one chloride anion in close proximity to H_a, H_g and H_c with relatively short contact distances ranging from 2.2 to 2.4 Å (Fig. 8B). It is interesting at this point to highlight the large difference observed between the curves plotted for both pyridinium protons H_f and H_c. This contrast is more evidence of the significant chelate effect promoting the binding of chloride between two positively charged pyridinium rings.

The solid-state structure of **2**·$(Cl)_4$ obtained by X-ray diffraction analysis is shown in Fig. 9. As seen on the ORTEP[57] views, the bis-viologen adopts a twisted configuration wherein both propyl-linked pyridine planes form an angle of $\sim 60^\circ$. The compact self-packing in the crystal lattice results in the observation of a wide range of 'short' contact distances (2.5 Å $\leq d \leq$ 3 Å) between all the hydrogen atoms in $\mathbf{2}^{4+}$ and chloride anions, water molecules or oxygen atoms from neighbouring $\mathbf{2}^{4+}$. This result confirms the ability of each pyridinium proton to establish strong interactions with hydrogen bond acceptors as halides. All four chloride atoms are at least complexed through two hydrogen bonds but the chelate effect revealed by ^{1}H-NMR is not clearly evidenced in the solid state. Such solid-state-specific behaviour has been attributed to strong packing effects favouring tight intermolecular associations leading to the self-assembled supramolecular stair-shaped arrangement shown in Fig. 9(C and D). The bis-viologen derivatives indeed form infinite accordion-like sheets wherein two consecutive (N4N5) viologens, linked through three chloride ions, form a 90° angle. Three aligned chloride anions, each complexed through four hydrogen bonds involving aromatic pyridinium protons, define the edge of this stair-shaped arrangement. The ^{1}H-NMR studies combined to theoretical calculations and solid-state analyses, thus clearly indicate the anion-binding ability of the bis-viologen receptor $\mathbf{2}^{4+}$ able to complex up to four anions in two distinct binding sites through a combination of hydrogen bonds and ion-pairing effects.

Due to their electron-deficient nature, viologens are known to form a wide range of charge-transfer complexes with electron-rich species.[77,78] Charge-transfer (CT) interactions between donors and acceptors are an important class of non-covalent interactions which have been greatly exploited in the design and synthesis of self-organizing systems, such as molecular tweezers and molecular clips.

The ability of $\mathbf{2}^{4+}$ to form such donor–acceptor complexes with halides was assessed in DMSO by absorption spectroscopy through the observation of charge-transfer bands in the UV-visible range. In agreement with its large electron density and high polarizability, only iodide turned out to produce a relatively intense color change, associated with a broad CT absorption band centered at $\sim$430 nm, in the presence of $\mathbf{2}^{4+}$ in DMSO. Addition of bromide did not yield clear additional bands but an overall increase in absorption below 450 nm, and no evidence of CT complex could be observed in the presence of chloride. This evolution agrees with the 'hard' nature of chloride resulting in weak donor–acceptor complexes characterized by high-energy CT transitions ($\lambda_{Cl}^{CT} < \lambda_{Br}^{CT} < \lambda_{I}^{CT}$). The exact stoichiometry of these associations could not be determined in solution using classical methods but the ability of iodide to form a CT complex with $\mathbf{2}^{4+}$ was further confirmed in the solid state by careful examination of the iodide positions in the crystal structure of [**2**·DMSO·$(I)_4$]. As is clearly shown

 This journal is © The Royal Society of Chemistry and the Centre National de la Recherche Scientifique 2010

View Online

Published on 28 May 2010 on http://pubs.rsc.org | doi:10.1039/B9NJ00757A
Downloaded by Technische Universitat Braunschweig on 21 October 2010

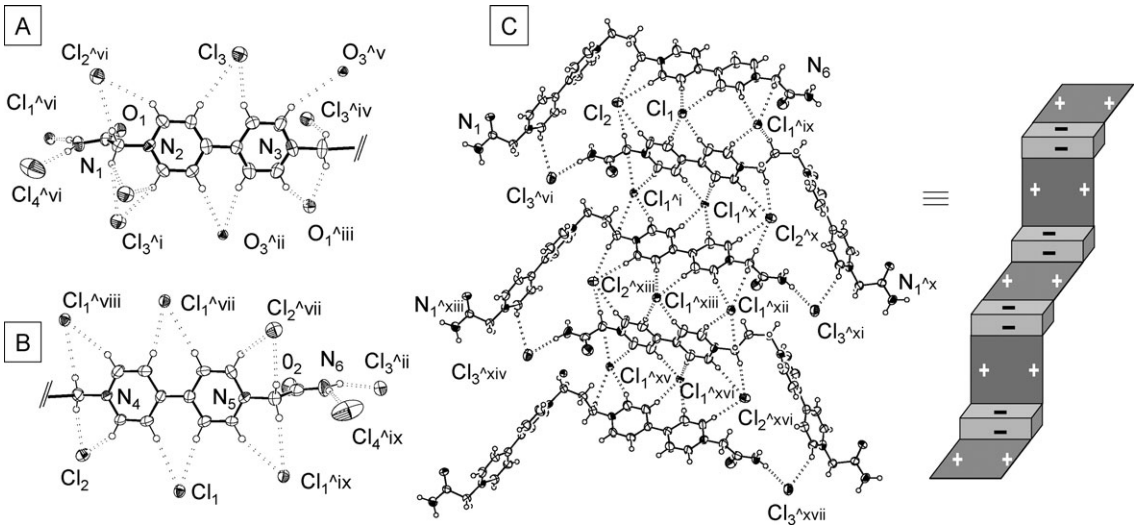

Fig. 9 ORTEP[57] views of $[\mathbf{2}\cdot(H_2O)_{0.5}\cdot(DMSO)_{0.55}\cdot(Cl)_4]$ showing the heteroatom-labelling scheme. (A) and (B) Detailed views of the chloride and oxygen atoms observed in short contact (2.5 Å $\leq d \leq$ 3 Å) with both viologen fragments in $\mathbf{2}^{4+}$. Each viologen is shown separately and the central carbon atom of the propyl linker has been omitted for clarity. (C) Partial view of the crystal packing. (D) Schematic drawing showing the stair-shaped arrangement observed in the solid state. Ellipsoids are drawn at a 45% probability level. The symmetry operations and translations used to generate all the represented atoms from the asymmetric unit are: (i) $((x + \frac{1}{2}) - 1, y + \frac{1}{2}, z)$; (ii) $(x + \frac{1}{2}, \frac{1}{2} - y, z + \frac{1}{2})$; (iii) $((\frac{1}{2} - x) + 1, \frac{1}{2} - y, (-z) + 1)$; (iv) $((-x) + 2, -y, (-z) + 1)$; (v) $(x + 1, -y, z + \frac{1}{2})$; (vi) $((-x) + 2, (-y) + 1, (-z) + 1)$; (vii) $((\frac{1}{2} - x) + 2, (\frac{1}{2} + y) - 1, (\frac{1}{2} - z) + 1)$; (viii) $((\frac{1}{2} + x) - 1, (\frac{1}{2} + y) - 1, z)$; (ix) $((-x) + 3, y, (\frac{1}{2} - z) + 1)$; (x) $((\frac{1}{2} - x) + 2, y + \frac{1}{2}, (\frac{1}{2} - z) + 1)$; (xi) $(\frac{1}{2} + x, (\frac{1}{2} - y) + 1, \frac{1}{2} + z)$; (xii) $((-x) + 3, y + 1, (\frac{1}{2} - z) + 1)$; (xiii) $(x, y + 1, z)$; (xiv) $((-x) + 2, (-y) + 2, (-z) + 1)$; (xv) $((\frac{1}{2} + x) - 1, (\frac{1}{2} + y) + 1, z)$; (xvi) $((\frac{1}{2} - x) + 2, (\frac{1}{2} + y) + 1, (\frac{1}{2} - z) + 1)$; (xvii) $(x + \frac{1}{2}, (\frac{1}{2} - y) + 2, z + \frac{1}{2})$.

in Fig. 10, viologens and iodides stack alternately to form an endless linear assembly. Two types of iodides, I_1 and I_2, are located between parallel viologen-based sheets with relatively short contact distances. The shortest, non-hydrogen-bond contact measured from I1 was found with N1, with d(I1–C10) = 3.9 Å and I1–Ĉ10–C3 ≈ 84°.

The particular case of fluoride

Among all the anionic species investigated, only fluoride could be clearly detected by the naked eye and by electrochemical

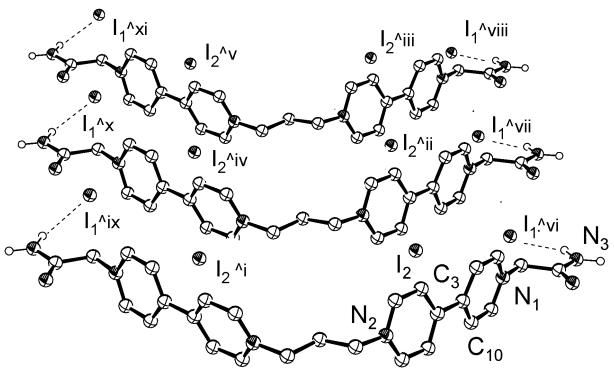

Fig. 10 ORTEP[57] views of $[\mathbf{2}\cdot DMSO\cdot(I)_4]$ showing the heteroatom-labelling scheme and the successive layers of iodides and viologens. Hydrogen atoms and solvent molecules have been omitted for clarity. Ellipsoids are drawn at a 45% probability level. The symmetry operations used to generate all the represented atoms from the asymmetric unit are: (i) $(-x, y, \frac{1}{2} - z)$; (ii) $(x, y - 1, z)$; (iii) $(x, y - 2, z)$; (iv) $(-x, y - 1, \frac{1}{2} - z)$; (v) $(-x, y - 2, \frac{1}{2} - z)$; (vi) $(-x, -y, -z)$; (vii) $(-x, (-y) - 1, -z)$; (viii) $(-x, (-y) - 2, -z)$. (ix) $(x, -y, z + \frac{1}{2})$; (x) $(x, (-y) - 1, z + \frac{1}{2})$; (xi) $(x, (-y) - 2, z + \frac{1}{2})$.

methods (see ESI†). This anion combines superlatives as it is the smallest, the most electronegative and most basic anion of the halides and plays well known crucial roles in numerous biological processes.[79] These pronounced features have already been exploited to develop fluoride chemosensors relying on size,[80–83] unusually strong H-bond[84–87] pK_a values[88–91] or unusual reactivities[92–95] for selectivity.

The addition of 0.2 molar equivalents of TBAF to a DMF solution of $\mathbf{1}\cdot(PF_6)_2$ or $\mathbf{2}\cdot(PF_6)_4$ induced drastic colour changes from colourless to intense blue or violet, respectively. From the spectro-electrochemical experiments described in the previous section, these signals were easily attributed to species in which viologen fragments have been reduced. The UV-vis spectrum of the blue solution obtained upon addition of fluoride to the mono-viologen $\mathbf{1}^{2+}$ indeed fully matches the signature observed in the course of the bulk electrochemical reduction conducted at −1 V. Addition of fluoride to a solution of $\mathbf{2}^{4+}$ led similarly to the development of signals attributed to the π-dimer $[\mathbf{2}^{2+}]_{dim}$ (Fig. 11)

These assumptions could be confirmed by electrochemical investigations carried out on solutions containing different ratios of fluoride anions and $\mathbf{2}\cdot(PF_6)_4$ or $\mathbf{1}\cdot(PF_6)_2$. The addition of aliquots of fluorides to a deoxygenated DMF solution of $\mathbf{1}^{2+}$ was followed by voltammetry with a rotating disk, and the formation of the reduced species was proved by the observation of a clear oxidation wave. After adding 1 molar equiv. of fluoride, the wave corresponding to the reduction of $\mathbf{1}^{2+}$ was almost completely transformed into a new diffusion wave attributed to the oxidation of $\mathbf{1}^{\bullet+}$ (Fig. 11). Similar results, demonstrating the formation of reduced viologens in the presence of fluoride, were obtained with $\mathbf{2}^{4+}$ as well as with the reference compound $\mathbf{4}^{2+}$. These results thus clearly demonstrate that the

View Online

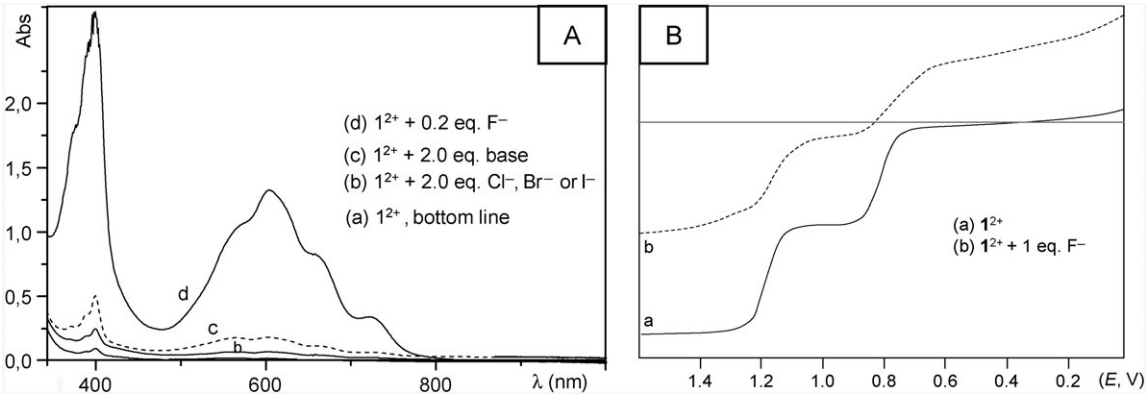

Fig. 11 (A) Absorption spectrum recorded for $\mathbf{1}\cdot(PF_6)_2$ (1 mM in DMF under argon atmosphere) upon addition of TBA^+ salt of F^- (0.2 molar equiv.) or Cl^-, Br^-, I^- and diisopropylamine (2 molar equiv.). (B) Voltammetric curves recorded with a rotating disk electrode before and after addition of TBAF to a DMF solution of 1 mM $\mathbf{1}\cdot(PF_6)_2$ (inside glove box).

Published on 28 May 2010 on http://pubs.rsc.org | doi:10.1039/B9NJ00757A
Downloaded by Technische Universitat Braunschweig on 21 October 2010

addition of fluoride leads to a reduction of the viologen fragments in DMF. A similar behaviour was also observed in DMSO. Given the "hard" nature of this anion, this electron transfer cannot reasonably be attributed to the oxidation of fluoride anion but instead to its mildly basic character. The addition of diisopropylamine, however, did not induce significant changes in the UV-vis spectrum. The exact mechanism leading to this intense color change is still unclear. It needs to be mentioned that the addition of an excess fluoride leads to the loss of the electrochemical and UV-visible signatures.

Theoretical calculation

In order to gain insights into the geometry of the π-dimerized bis-viologen species $[\mathbf{2}^{2+}]_{dim}$ and into the associated dynamic process, theoretical calculations were undertaken using various levels of calculation, namely DFT, DFT-D, DFT-CP and MP2. The π-dimer $[\mathbf{2}^{2+}]_{dim}$ is expected to develop intramolecular interactions mostly driven by dispersion energy. This contribution is computationally demanding and if MP2 is well known to give a proper description of the dispersion energy, it is also well known that a large basis set is mandatory. In order to include this dispersion energy at a lower cost, we also used the DFT-D[50] and DFT-CP[39] levels of calculations (full computational details are given in the ESI†). These levels have already been used for large molecular systems[96,97] with an important contribution of the dispersion energy. For comparison purpose, DFT calculations using the BLYP and B3LYP functionals were also performed.

We focused primarily on the non-reduced starting material $\mathbf{2}^{4+}$, whose structure could be obtained through geometry optimization. In accordance with the existence of electrostatic repulsion forces driving both doubly charged viologens away from each other, our calculations always lead to an open structure. As discussed in the previous section, this species was also characterized in the solid state by X-ray diffraction analysis in the presence of chloride or iodide anions (Fig. 9 and 10). The agreement of our calculations with these X-ray data is good (Table 2), and we found that the amplitude of the torsion angle γ measured for C7–C8–C11–C12 (Table 3), defining the tilt angle between both pyridines in each viologen fragment, depends on the nature of the counter-anion. We also found that the torsional angle γ observed on the optimized structure of $\mathbf{2}^{4+}$ in the absence of counter-anions is close to that measured experimentally (~31°) on the solid-state structure of $\mathbf{1}\cdot(PF_6)_2$. In contrast, the same angle estimated theoretically with $\mathbf{2}^{4+}$ in interaction with two iodine anions matches that measured (~13°) on the X-ray structure of the bis-viologen derivative $[\mathbf{2}\cdot DMSO\cdot(I)_4]$. These differences thus indicate that the tilt angle is high with non-interacting anions such as PF_6^- but it gets significantly reduced by the CT process established with iodide. Moreover, the comparison between $\mathbf{2}^{4+}$ and the simple *N*-methylated derivative $\mathbf{4}^{2+}$ demonstrates that the amide terminal group has no influence on the geometry of the viologen units.[98] The singlet state of the bis-viologen $\mathbf{2}^{4+}$ was found to be the ground state of the molecule, since the singlet state is 61.8 or 58.6 kcal mol^{-1} lower than the triplet state at the B3LYP/6-31+G** and the B3LYP−CP/6-31+G**, respectively.

The theoretical description of the doubly reduced $\mathbf{2}^{2+}$ species is trickier. Both the open $[\mathbf{2}^{2+}]_{open}$ and the closed π-dimer $[\mathbf{2}^{2+}]_{dim}$ forms can be characterized, and frequency calculations confirm that both of them are minima on the PES (Potential Energy Surface). The singlet and triplet spin states have been investigated for each form.[99]

In the optimized open structure $[\mathbf{2}^{2+}]_{open}$, we found that the torsion angle γ measured between both pyridine fragments (C7–C8–C11–C12) in each viologen was around 5.0° whatever the spin state being considered. This small value, defining a nearly coplanar arrangement, is in accordance with our assumption that the tilt angle γ strongly decreases when the electron density on the viologen increases, as seen by electrochemical reduction or through the formation of a CT complex with electron-rich iodide anions.[100]

The singlet and triplet states of the closed π-dimer structures $[\mathbf{2}^{2+}]_{dim}$ show significant structural differences. The singlet-state closed-form $^{S}[\mathbf{2}^{2+}]_{dim}$ exhibits a geometry wherein both viologen units are almost perfectly parallel (Table 3, α ~ 4–5°), whereas a significantly more open structure was found in the triplet state $^{T}[\mathbf{2}^{2+}]_{dim}$ (α ~ 15°) (see Table 3). Due to the important size of the viologen units, this 10° deviation measured

 This journal is © The Royal Society of Chemistry and the Centre National de la Recherche Scientifique 2010

View Online

Table 2 Comparison between structural parameters defining $\mathbf{2}^{4+}$ obtained by theoretical calculation and X-ray diffraction analyses. Distances and angles are given in Å and degrees, respectively

	X-ray diffraction data		B3LYP/6-31+G**	B3LYP–CP/6-31+G**	B3LYP/6-31+G**	PBE0/6-311G** (ref. 98)
	$\mathbf{1}\cdot(PF_6)_2$	$[\mathbf{2}\cdot DMSO\cdot(I)_4]$	$[\mathbf{2}^{4+}]_{open}$	$[\mathbf{2}^{4+}]_{open}$	$[\mathbf{2}^{4+}]_{open}\cdot(I^-)_2$	$\mathbf{4}^{2+}$
N1–C2	1.315	1.347	1.339	1.338	1.351	—
C2–O3	1.220	1.227	1.224	1.225	1.221	—
C2–C4	1.518	1.503	1.564	1.559	1.551	—
C4–N5	1.460	1.449	1.477	1.470	1.470	1.491
N5–C6	1.349	1.329	1.354	1.351	1.364	1.351
C6–C7	1.381	1.385	1.389	1.387	1.371	1.382
C7–C8	1.376	1.367	1.401	1.396	1.418	1.401
C8–C11	1.481	1.493	1.491	1.480	1.487	1.488
C11–C12	1.404	1.346	1.409	1.404	1.426	—
C12–C13	1.382	1.387	1.384	1.381	1.369	—
C13–N14	1.318	1.335	1.359	1.355	1.366	—
N14–C17	1.478	1.474	1.498	1.490	1.475	—
C17–C18–C19	—	112.4	108.1	107.8	110.9	—
C7–C8–C11–C12	31.0	13.0	38.6	38.1	11.1	43.0

Table 3 Geometrical parameters calculated for the reduced π-dimer $[\mathbf{2}^{2+}]_{dim}$ conformations in the singlet ($^S[\mathbf{2}^{2+}]_{dim}$) or triplet state ($^T[\mathbf{2}^{2+}]_{dim}$) using the B3LYP/6-31+G** or B3LYP–CP/6-31+G** calculation levels. The distances are given in Å; angles are given in degrees. For the definition of the atom labels, see Fig. 7. The optimized structure shown corresponds to the closed conformation found for the triplet state $^T[\mathbf{2}^{2+}]_{dim}$

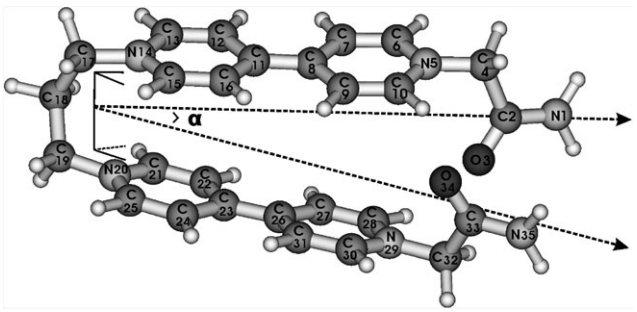

	B3LYP/6-31+G**		B3LYP–CP/6-31+G**	
	$^S[\mathbf{2}^{2+}]_{dim}$	$^T[\mathbf{2}^{2+}]_{dim}$	$^S[\mathbf{2}^{2+}]_{dim}$	$^T[\mathbf{2}^{2+}]_{dim}$
C4–N5	1.464	1.460	1.457	1.455
N5–C6	1.369	1.373	1.363	1.366
C6–C7	1.369	1.367	1.365	1.365
C7–C8	1.431	1.433	1.424	1.426
C8–C11	1.436	1.433	1.426	1.426
C23–C26	1.436	1.433	1.427	1.425
N14–N20	3.007	3.296	2.891	3.041
N5–N29	4.153	5.556	3.678	4.589
C7–C8–C11–C12	5.3	6.1	0.9	3.3
α	5.1	18.0	5.2	13.1

between the triplet and singlet states leads to a difference of 1 Å in the N5–N29 distance and to a smaller shift of 0.2 Å for N14–N20 (Table 3).

The molecular orbital analyses of the singlet states of $\mathbf{2}^{2+}$ in the closed and open conformations are shown in Fig. 12. The LUMO (Lowest Unoccupied Molecular Orbital) of the open starting material $\mathbf{2}^{4+}$ becomes the HOMO (Highest Occupied Molecular Orbital) of the doubly reduced $\mathbf{2}^{2+}$ species with a bonding character associated to the C8–C11 (C23–C26) bonds. The same bonding character was observed for the C7–C6 (C9–C10) and C13–C12 (C15–C16) bonds, whereas an antibonding character is associated to the C7–C8 (C8–C9), N5–C6 (N5–C10) and N14–C13 (N14–C15) bonds. The electron-doping process has thus significant consequences on the geometry of the viologen units as shown by the differences observed between the bond distances tabulated in Table 2 and 3. Reducing $\mathbf{2}^{4+}$ into $\mathbf{2}^{2+}$ led especially to significant bond lengths increases for N5–C6 (N5–C10), C7–C8 (C9–C8) and to the concomitant decreases of the C8–C11, C6–C7 (C9–C10) bond distances. As seen on Fig. 12, the HOMO of $\mathbf{2}^{2+}$ is also clearly responsible for the association between both viologen fragment forming the closed π-dimer $[\mathbf{2}^{2+}]_{dim}$ species.

From an energetic point of view, the difference in energy between the open and π-dimer forms of the doubly reduced $\mathbf{2}^{2+}$ species proved to be highly sensitive to the chosen level of calculations (Table 4). A previously reported ESR investigation conducted with a simple bisalkylated viologen[101] V^{2+}, established that the singlet state of the reduced form $^S[V^{\bullet+}]$ is more stable at low temperature (around 100 K), whereas the triplet state $^T[V^{\bullet+}]$ was only detected at room temperature. From these experiments, it was postulated that the singlet state π-dimer $^S[(V)_2{}^{2+}]_{dim}$ is more stable at low temperature. In contrast, the spectrum recorded at room temperature confirmed the presence of unpaired electrons attributed to $[V]^{\bullet+}$ with a weak contribution corresponding to the triplet dimer $^T[(V_2)^{2+}]_{dim}$. Similar behaviours were observed with various viologen-based radicals[14] becoming ESR silent at low temperatures. Such temperature-dependent loss of ESR signal was also frequently interpreted as a diagnostic signature of the π-dimerization process assuming the formation of bis-radical spin-paired dimers at low temperatures and of non-associated radicals at RT. In the case of $\mathbf{2}^{4+}$, the situation is much more complex since the dimerization is an intramolecular process wherein the opening of the singlet state dimerized closed structure $^S[\mathbf{2}^{2+}]_{dim}$ could lead to electron unpairing to produce the $^T[\mathbf{2}^{2+}]_{open}$ or could keep its spin state through the opening process to generate an ESR-silent $^S[\mathbf{2}^{2+}]_{open}$ species.

At the widely used B3LYP/6-31+G** calculation level, the closed conformation in the singlet state $^S[\mathbf{2}^{2+}]_{dim}$ is slightly more stable than its corresponding open singlet structure

Downloaded by Technische Universitat Braunschweig on 21 October 2010
Published on 28 May 2010 on http://pubs.rsc.org | doi:10.1039/B9NJ00757A

View Online

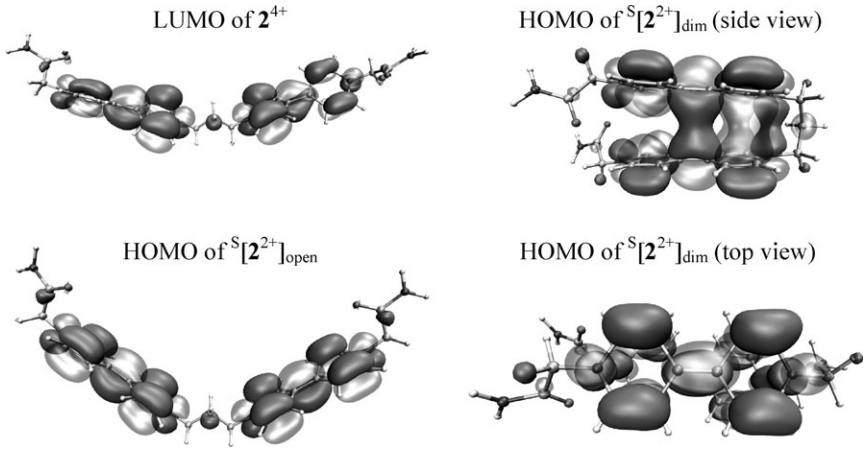

Fig. 12 Selected molecular orbitals obtained for the singlet states of $\mathbf{2}^{4+}$ and $\mathbf{2}^{2+}$ in closed ($^{S}[\mathbf{2}^{2+}]_{dim}$) and open ($^{S}[\mathbf{2}^{2+}]_{open}$) conformations. The electron density isosurface is 0.02 a.u.

Table 4 Relative energy differences between the singlet (S) and triplet (T) states of the closed and open conformation calculated for $\mathbf{2}^{2+}$. The closed $[\mathbf{2}^{2+}]_{dim}$ conformation is favored when $\Delta E < 0$

Method	ΔE/kcal mol^{-1}	Spin state
B3LYP/6-31+G**	−0.9	S
B3LYP/6-31+G**	+6.6	T
B3LYP−CP/6-31+G**	−21.7	S
B3LYP−CP/6-31+G**	−3.2	T
B3LYP−CP/6-31+G**+water	−25.0	S
B3LYP/6-31+G** + water	−2.8	S
B3LYP/6-31+G** + acetonitrile	−3.4	S
MP2/6-31+G**//B3LYP-CP/6-31+G**	−9.5	S
PBE/DZVP-GTH	−3.4	S
PBE−D/DZVP-GTH	−23.0	S
PBE/DZVP-GTH	+7.2	T
PBE−D/DZVP-GTH	−1.8	T
BLYP/6-31+G(d,p)	+6.6	S
BLYP/DZVP-GTH	+8.9	S
BLYP−D/DZVP-GTH	−12.1	S

$^{S}[\mathbf{2}^{2+}]_{open}$ with a stabilization of 0.9 kcal mol^{-1}. As seen in values reported in Table 4, the inclusion of dispersion energy, through various methods involving dispersion terms or corrected potentials, clearly favours the closed conformation. The inclusion of water as solvent through PCM models[43–46] also turned out to favour the closed form, although at a lesser extent. In contrast, the BLYP functional proved to favour the open structure with energy differences of 6.6 kcal mol^{-1} and 8.9 kcal mol^{-1} with the 6-31+G** and DZVP-GTH basis sets, respectively. But the inclusion of dispersion energy with BLYP−D/DZVP-GTH also led to the stabilization of the π-dimer form with an energy difference of 12.1 kcal mol^{-1}.

As expected, the triplet state systematically favoured the open structure. For example, the open structure was found to be more stable by 6.6 kcal mol^{-1} and 7.2 kcal mol^{-1} at the B3LYP/6-31+G** and PBE/DZVP levels of calculation, respectively. The inclusion of dispersion contributions with corrected potentials also led to the stabilization of the closed conformation by 3.2 kcal mol^{-1} and 1.8 kcal mol^{-1} with B3LYP-CP/6-31G** and PBE-D/DZVP, respectively. Finally, it should be noted that at the B3LYP/6-31+G** level, the triplet state turned out to be more stable in both the open and closed conformations whereas at the B3LYP−CP/6-31+G** level, the singlet state of the closed conformation was the more stable, in agreement with the ESR experimental data.

In conclusion, this theoretical investigation shows the utmost importance of dispersion energy in the modelisation of π-dimers. This inclusion of dispersion energy and its effects through the use of dispersion terms or corrected potentials in conjunction with DFT methods proved to favour the closed structure $[\mathbf{2}^{2+}]_{dim}$ whatever the spin state considered or the functional used. Due to the structure of $[\mathbf{2}^{2+}]_{dim}$, there is no doubt about the importance of dispersion terms and about their necessity beyond the DFT level of theory.[102] Thus, a preference for the dimeric structure in the singlet state can be deduced from our theoretical investigations, but the observation of the open structure as a minimum on the PES led us to assume that interconversion between the two conformations has to be considered.

Finally, using metadynamics[55,56,103] with the N–N distances as collective variables, we have been able to estimate the free energy barrier required to switch the closed singlet state $[\mathbf{2}^{2+}]_{dim}$ into the open non-associated structure at around 8 kcal mol^{-1} at 300 K at the BLYP−D/DZVP-GTH calculation level.

Conclusion

Electron-deficient viologens are unique molecular materials finding potential applications in numerous arenas ranging from agriculture to nanosciences. In this study, we have established that the association of two viologen fragments through a propyl linker promotes an original chelate-like complexation of chloride anions in polar DMSO–H_2O media. The solid-state X-ray analyses of the chloride and iodide complexes further revealed the large range of non-covalent interactions potentially displayed by viologen-based anion receptors. In the crystal lattice, chlorides were found to be complexed through a dense hydrogen bond network whereas the location of iodides in the crystal was found to be driven by CT processes with the electron-deficient pyridinium rings. Among all the anionic species investigated, only fluoride could be clearly detected by naked eyes and by electrochemical methods. The reduction-triggered formation of a π-dimer from two viologen-based cation radicals was moreover investigated

Downloaded by Technische Universitat Braunschweig on 21 October 2010
Published on 28 May 2010 on http://pubs.rsc.org | doi:10.1039/B9NJ00757A

 This journal is © The Royal Society of Chemistry and the Centre National de la Recherche Scientifique 2010

View Online

by electrochemical and spectroelectrochemical methods and by theoretical calculation. The latter were performed at the DFT, DFT-D and DFT-CP MP2 calculation levels and allowed us to obtain essential structural information on the singlet- and triplet-state π-dimerized bis-viologen $[2^{2+}]_{dim}$ species.

Acknowledgements

The authors gratefully acknowledge the ANR (PCV e-bioprob) for financial support and Christian Philouze for the X-Ray diffraction analyses. AM and MO gratefully acknowledge the CECIC center for computer facilities.

Published on 28 May 2010 on http://pubs.rsc.org | doi:10.1039/B9NJ00757A
Downloaded by Technische Universitat Braunschweig on 21 October 2010

References

1 J. L. Sessler, P. A. Gale and W.-S. Cho, *Anion Receptor Chemistry*, RSC, Cambridge, 2006.
2 P. A. Gale, S. E. Garcia-Garrido and J. Garric, *Chem. Soc. Rev.*, 2008, **37**, 151.
3 P. D. Beer and S. R. Bayly, *Top. Curr. Chem.*, 2005, **255**, 125.
4 F. P. Schmidtchen, in *Supramolecular Chemistry of Anions*, ed. A. Bianchi, K. Bowman-James and E. Garcia-Espana, Wiley-VCH, 1998, p. 284.
5 H. G. Loehr and F. Voegtle, *Acc. Chem. Res.*, 1985, **18**, 65.
6 C. Suksai and T. Tuntulani, *Chem. Soc. Rev.*, 2003, **32**, 192.
7 D. Curiel, E. J. Hayes and P. D. Beer, in *Topics in Fluorescence Spectroscopy; Advanced Concepts in Fluorescence Sensing, Part A*, ed. C. D. Geddes and J. R. Lakowicz, Springer-Verlag, New York, 2005, p. 59.
8 C. Bucher, C. H. Devillers, J.-C. Moutet, G. Royal and E. Saint-Aman, *New J. Chem.*, 2004, **28**, 1584.
9 C. Bucher, C. H. Devillers, J.-C. Moutet, J. Pécaut, G. Royal, E. Saint-Aman and F. Thomas, *Dalton Trans.*, 2005, 3620.
10 O. Reynes, C. Bucher, J.-C. Moutet, G. Royal, E. Saint-Aman and E.-M. Ungureanu, *J. Electroanal. Chem.*, 2005, **580**, 291.
11 C. Bucher, C. H. Devillers, J.-C. Moutet, G. Royal and E. Saint-Aman, *Coord. Chem. Rev.*, 2009, **253**, 21.
12 P. D. Beer, P. A. Gale and G. Z. Chen, *J. Chem. Soc., Dalton Trans.*, 1999, 1897.
13 E. García-España, P. Díaz, J. M. Llinares and A. Bianchi, *Coord. Chem. Rev.*, 2006, **250**, 2952.
14 P. M. S. Monk, *The Viologens: Physicochemical Properties, Synthesis and Applications of the Salts of 4,4′-Bipyridine*, Wiley, 1998.
15 D. B. Amabilino, F. M. Raymo and J. F. Stoddart, in *Comprehensive Supramolecular Chemistry*, ed. J.-P. Sauvage and M. W. Hosseini, Pergamon, 1996, p. 85.
16 C. G. Claessens and J. F. Stoddart, *J. Phys. Org. Chem.*, 1997, **10**, 254.
17 S. J. Dickson, E. V. B. Wallace, A. N. Swinburne, M. J. Paterson, G. O. Lloyd, A. Beeby, W. J. Belcher and J. W. Steed, *New J. Chem.*, 2008, **32**, 786.
18 A. R. Bernardo, J. F. Stoddart and A. E. Kaifer, *J. Am. Chem. Soc.*, 1992, **114**, 10624.
19 M. T. Rojas and A. E. Kaifer, *J. Am. Chem. Soc.*, 1995, **117**, 5883.
20 O. Reynes, C. Bucher, J.-C. Moutet, G. Royal and E. Saint-Aman, *Chem. Commun.*, 2004, 428.
21 E. A. Smith, R. R. Lilienthal, R. J. Fonseca and D. K. Smith, *Anal. Chem.*, 1994, **66**, 3013.
22 H. T. van Dam and J. J. Ponjeé, *J. Electrochem. Soc.*, 1974, **121**, 1555.
23 T. Sagara, H. Tsuruta and N. Nakashima, *J. Electroanal. Chem.*, 2001, **500**, 255.
24 H. Kunkely and A. Vogler, *Chem. Phys. Lett.*, 2001, **345**, 309.
25 K. Kamata, T. Suzuki, T. Kawai and T. Iyoda, *J. Electroanal. Chem.*, 1999, **473**, 145.
26 A. Y. Ziganshina, S. V. Kharlamov, D. E. Korshin, R. K. Mukhitova, E. K. Kazakova, S. K. Latypov, V. V. Yanilkin and A. I. Konovalov, *Tetrahedron Lett.*, 2008, **49**, 5312.
27 T. Sata, Y. Matsuo, T. Yamaguchi and K. Matsusaki, *J. Chem. Soc., Faraday Trans.*, 1997, **93**, 2553.
28 I. Giner, G. Pera, C. Lafuente, M. C. Lopez and P. Cea, *J. Colloid Interface Sci.*, 2007, **315**, 588.
29 T. Sagara, H. Maeda, Y. Yuan and N. Nakashima, *Langmuir*, 1999, **15**, 3823.
30 H. C. De Long and D. A. Buttry, *Langmuir*, 1990, **6**, 1319.
31 K. Kamata, T. Kawai and T. Iyoda, *Langmuir*, 2001, **17**, 155.
32 T. Komura, T. Yamaguchi, K. Sirono and K. Kura, *Electroanalysis*, 2002, **14**, 823.
33 A. Schiller, B. Vilozny, R. A. Wessling and B. Singaram, *Anal. Chim. Acta*, 2008, **627**, 203.
34 Y. S. Park, E. J. Lee, Y. S. Chun, Y. D. Yoon and K. B. Yoon, *J. Am. Chem. Soc.*, 2002, **124**, 7123.
35 B. L. Allwood, N. Spencer, H. Shahriari-Zavareh, J. F. Stoddart and D. J. Williams, *J. Chem. Soc., Chem. Commun.*, 1987, 1064.
36 K. Sakai, Y. Ikuta, M. Shiomi, T. Tamane, Y. Tomita, T. Tsubomura and N. Nemoto, *Acta Crystallogr., Sect. C: Cryst. Struct. Commun.*, 1997, **53**, 331.
37 M. J. Frisch, G. W. Trucks, H. B. Schlegel, G. E. Scuseria, M. A. Robb, J. R. Cheeseman, J. Montgomery, J. A., T. Vreven, K. N. Kudin, J. C. Burant, J. M. Millam, S. S. Iyengar, J. Tomasi, V. Barone, B. Mennucci, M. Cossi, G. Scalmani, N. Rega, G. A. Petersson, H. Nakatsuji, M. Hada, M. Ehara, K. Toyota, R. Fukuda, J. Hasegawa, M. Ishida, T. Nakajima, Y. Honda, O. Kitao, H. Nakai, M. Klene, X. Li, J. E. Knox, H. P. Hratchian, J. B. Cross, V. Bakken, C. Adamo, J. Jaramillo, R. Gomperts, R. E. Stratmann, O. Yazyev, A. J. Austin, R. Cammi, C. Pomelli, J. W. Ochterski, P. Y. Ayala, K. Morokuma, G. A. Voth, P. Salvador, J. J. Dannenberg, V. G. Zakrzewski, S. Dapprich, A. D. Daniels, M. C. Strain, O. Farkas, D. K. Malick, A. D. Rabuck, K. Raghavachari, J. B. Foresman, J. V. Ortiz, Q. Cui, A. G. Baboul, S. Clifford, J. Cioslowski, B. B. Stefanov, G. Liu, A. Liashenko, P. Piskorz, I. Komaromi, R. L. Martin, D. J. Fox, T. Keith, M. A. Al-Laham, C. Y. Peng, A. Nanayakkara, M. Challacombe, P. M. W. Gill, B. Johnson, W. Chen, M. W. Wong, C. Gonzalez and J. A. Pople, *GAUSSIAN 03 (Revision C.02)*, Gaussian, Inc., Wallingford, CT, 2004.
38 A. D. Becke, *J. Chem. Phys.*, 1993, **98**, 5648.
39 G. A. DiLabio, *Chem. Phys. Lett.*, 2008, **455**, 348.
40 C. Moller and M. S. Plesset, *Phys. Rev.*, 1934, **46**, 618.
41 M. J. Frisch, J. A. Pople and J. S. Binkley, *J. Chem. Phys.*, 1984, **80**, 3265.
42 T. Clark, J. Chandrasekhar, G. W. Spitznagel and P. V. R. Schleyer, *J. Comput. Chem.*, 1983, **4**, 294.
43 M. T. Cancès, B. Mennucci and J. Tomasi, *J. Chem. Phys.*, 1997, **107**, 3032.
44 M. Cossi, V. Barone, B. Mennucci and J. Tomasi, *Chem. Phys. Lett.*, 1998, **286**, 253.
45 B. Mennucci and J. Tomasi, *J. Chem. Phys.*, 1997, **106**, 5151.
46 M. Cossi, G. Scalmani, N. Rega and V. Barone, *J. Chem. Phys.*, 2002, **117**, 43.
47 J. VandeVondele, M. Krack, F. Mohamed, M. Parrinello, T. Chassaing and J. Hutter, *Comput. Phys. Commun.*, 2005, **167**, 103.
48 A. D. Becke, *Phys. Rev. A: At., Mol., Opt. Phys.*, 1988, **38**, 3098.
49 C. T. Lee, W. T. Yang and R. G. Parr, *Phys. Rev. B: Condens. Matter*, 1988, **37**, 785.
50 J. S. Grimme, *J. Comput. Chem.*, 2006, **27**, 1787.
51 J. VandeVondele and J. Hutter, *J. Chem. Phys.*, 2007, **127**, 114105.
52 S. Goedecker, M. Teter and J. Hutter, *Phys. Rev. B: Condens. Matter*, 1996, **54**, 1703.
53 C. Hartwigsen, S. Goedecker and J. Hutter, *Phys. Rev. B: Condens. Matter Mater. Phys.*, 1998, **58**, 3641.
54 M. Krack, *Theor. Chem. Acc.*, 2005, **114**, 145.
55 A. Laio and M. Parrinello, *Proc. Natl. Acad. Sci. U. S. A.*, 2002, **99**, 12562.
56 C. Michel, A. Laio, F. Mahomed, M. Krack, M. Parrinello and A. Milet, *Organometallics*, 2007, **26**, 1241.
57 L. J. Farrugia, *J. Appl. Crystallogr.*, 1997, **30**, 565.
58 A. J. Bard, *Pure Appl. Chem.*, 1971, **25**, 379.
59 F. Ammar and J. M. Saveant, *J. Electroanal. Chem.*, 1973, **47**, 115.

View Online

60 J.-M. Lu, S. V. Rosokha and J. K. Kochi, *J. Am. Chem. Soc.*, 2003, **125**, 12161.
61 T. Nishinaga and K. Komatsu, *Org. Biomol. Chem.*, 2005, **3**, 561.
62 K. Lee, C. Lee, J. W. Park, Y. S. Park and K. B. Yoon, *Bull. Korean Chem. Soc.*, 1999, **20**, 1365.
63 E. M. Kosower and J. L. Cotter, *J. Am. Chem. Soc.*, 1964, **86**, 5524.
64 W. Geuder, S. Huenig and A. Suchy, *Tetrahedron*, 1986, **42**, 1665.
65 S. J. Atherton, K. Tsukahara and R. G. Wilkins, *J. Am. Chem. Soc.*, 1986, **108**, 3380.
66 M. Furue and S.-I. Nozakura, *Chem. Lett.*, 1980, 821.
67 N. Pedatsur, M.-C. Richoux and A. Harriman, *J. Chem. Soc., Faraday Trans. 2*, 1985, **81**, 1427.
68 A. Deronzier, B. Galland and E. Viera, *Nouv. J. Chim.*, 1982, **6**, 97.
69 D. E. Richardson and H. Taube, *Inorg. Chem.*, 1981, **20**, 1278.
70 C. Lee, Y. M. Lee, M. S. Moon, S. H. Park, J. W. Park, K. G. Kim and S.-J. Jeon, *J. Electroanal. Chem.*, 1996, **416**, 139.
71 P. D. Beer and P. A. Gale, *Angew. Chem., Int. Ed.*, 2001, **40**, 486.
72 D. Astruc, C. Ornelas and J. Ruiz, *Acc. Chem. Res.*, 2008, **41**, 841.
73 G. R. Desiraju and T. Steiner, *The Weak Hydrogen Bond*, Oxford University Press, New York, 1999.
74 K. A. Connors, *Binding Constants, The Measurement of Molecular Complex Stability*, John Wiley & Sons, New York, 1987.
75 M. T. Blanda, J. H. Horner and M. Newcom, *J. Org. Chem.*, 1989, **54**, 4626.
76 L. Fielding, *Tetrahedron*, 2000, **56**, 6151.
77 S. K. Lee, S. Y. Shin, S. Lee, C. Lee and J. W. Park, *J. Chem. Soc., Perkin Trans. 2*, 2001, **10**, 1983.
78 A. Deronzier and F. Esposito, *New J. Chem.*, 1983, **7**, 15.
79 K. L. Kirk, *Biochemistry of the Elemental Halogens and Inorganic Halides*, Plenum Press, New-York, 1991.
80 M. Takeuchi, T. Shioya and T. M. Swager, *Angew. Chem., Int. Ed.*, 2001, **40**, 3372.
81 S. Camiolo, P. A. Gale, M. B. Hursthouse and M. E. Light, *Org. Biomol. Chem.*, 2003, **1**, 741.
82 S. Camiolo and P. A. Gale, *Chem. Commun.*, 2000, 1129.
83 H. Miyaji and J. L. Sessler, *Angew. Chem., Int. Ed. Engl.*, 2001, 40.
84 J. Y. Kwon, Y. J. Jang, S. K. Kim, K.-H. Lee, J. S. Kim and J. Yoon, *J. Org. Chem.*, 2004, **69**, 5155.
85 S. K. Kim, J. H. Bok, R. A. Bartsch, J. Y. Lee and J. S. Kim, *Org. Lett.*, 2005, **7**, 4839.
86 M. Boiocchi, L. Del Boca, D. E. Gomez, L. Fabbrizzi, M. Licchelli and E. Monzani, *J. Am. Chem. Soc.*, 2004, **126**, 16507.
87 E. J. Cho, J. W. Moon, S. W. Ko, J. Y. Lee, S. K. Kim, J. Yoon and K. C. Nam, *J. Am. Chem. Soc.*, 2003, **125**, 12376.
88 T. Gunnlaugsson, P. E. Kruger, P. Jensen, F. M. Pfeffer and G. M. Hussey, *Tetrahedron Lett.*, 2003, **44**, 8909.
89 Z.-h. Lin, Y.-g. Zhao, C.-y. Duan, B.-g. Zhang and Z.-p. Bai, *Dalton Trans.*, 2006, 3678.
90 X. Peng, Y. Wu, J. Fan, M. Tian and K. Han, *J. Org. Chem.*, 2005, **70**, 10524.
91 T. Mizuno, W.-H. Wei, L. R. Eller and J. L. Sessler, *J. Am. Chem. Soc.*, 2002, **124**, 1134.
92 H. Yamamoto, A. Ori, K. Ueda, C. Dusemund and S. Shinkai, *Chem. Commun.*, 1996, 407.
93 X. Y. Liu, D. R. Bai and S. Wang, *Angew. Chem., Int. Ed.*, 2006, **45**, 5475.
94 S. J. M. Koskela, T. M. Fyles and T. D. James, *Chem. Commun.*, 2005, 945.
95 J. K. Day, C. Bresner, N. D. Coombs, I. A. Fallis, L.-L. Ooi and S. Aldridge, *Inorg. Chem.*, 2008, **47**, 793.
96 A. Ben Fredj, Z. Ben Lakhdar and M. F. Ruiz-Lopez, *Chem. Phys. Lett.*, 2009, **472**, 243.
97 I. D. Mackie and G. A. DiLabio, *J. Phys. Chem. A*, 2008, **112**, 10968.
98 A. Di Matteo, *Chem. Phys. Lett.*, 2007, **439**, 190.
99 Broken symmetry calculations have also been attempted with or without unsymmetrical starting geometry, but the symmetrical singlet state was always found to be the converged state.
100 G. Saielli, *J. Phys. Chem. A*, 2008, **112**, 7987.
101 C. Femoni, M. C. Iapalucci, G. Longoni, C. Tiozzo, J. Wolowska, S. Zacchini and E. Zazzaroni, *Chem. Eur. J.*, 2007, **13**, 6544.
102 A. Milet, T. Korona, R. Moszynski and E. Kochanski, *J. Chem. Phys.*, 1999, **111**, 7727.
103 A. Laio and F. L. Gervasio, *Rep. Prog. Phys.*, 2008, **71**, 126601.

Published on 28 May 2010 on http://pubs.rsc.org | doi:10.1039/B9NJ00757A
Downloaded by Technische Universitat Braunschweig on 21 October 2010

 This journal is © The Royal Society of Chemistry and the Centre National de la Recherche Scientifique 2010